Proteins: Structure, Function, and Bioinformatics

WILEY

PROTEINS

RESEARCH ARTICLE

Unraveling the Structural Basis of Biased Agonism in the β_2-Adrenergic Receptor Through Molecular Dynamics Simulations

Wojciech Plazinski[1,2] | Aneta Archala[1] | Krzysztof Jozwiak[1] | Anita Plazinska[1]

[1]Department of Biopharmacy, Medical University of Lublin, Lublin, Poland | [2]Jerzy Haber Institute of Catalysis and Surface Chemistry, Polish Academy of Sciences, Poland

Correspondence: Wojciech Plazinski (wojtek_plazinski@o2.pl) | Anita Plazinska (anita.plazinska@umlub.pl)

Received: 6 July 2024 | **Revised:** 17 October 2024 | **Accepted:** 1 November 2024

Funding: This work was supported by Narodowe Centrum Nauki and the National Science Centre, Poland [2017/25/B/NZ7/02654].

Keywords: biased agonism | molecular conformation | molecular dynamics | stereoselective effects | β_2-adrenergic receptor

ABSTRACT

Biased agonism in G protein-coupled receptors is a phenomenon resulting in the selective activation of distinct intracellular signaling pathways by different agonists, which may exhibit bias toward either Gs, Gi, or arrestin-mediated pathways. This study investigates the structural basis of ligand-induced biased agonism within the context of the β_2-adrenergic receptor (β_2-AR). Atomistic molecular dynamics simulations were conducted for β_2-AR complexes with two stereoisomers of methoxynaphtyl fenoterol (MNFen), that is, compounds eliciting qualitatively different cellular responses. The simulations reveal distinct interaction patterns within the binding cavity, dependent on the stereoisomer. These changes propagate to the intracellular parts of the receptor, triggering various structural responses: the dynamic structure of the intracellular regions of the (R,R)-MNFen complex more closely resembles the "G_s-compatible" and "β-arrestin-compatible" conformation of β_2-AR, while both stereoisomers maintain structural responses equidistant from the inactive conformation. These findings are confirmed by independent coarse-grained simulations. In the context of deciphered molecular mechanisms, Trp313 plays a pivotal role, altering its orientation upon interactions with (R,R)-MNFen, along with the Lys305-Asp192 ionic bridge. This effect, accompanied by ligand interactions with residues on TM2, increases the strength of interactions within the extracellular region and the binding cavity, resulting in a slightly more open conformation and a minor (by ca. 0.2 nm) increase in the distance between the TM5–TM7, TM1–TM6, TM6–TM7, and TM1–TM5 pairs. On the other hand, an even slighter decrease in the distance between the TM1–TM4 and TM2–TM4 pairs is observed.

1 | Introduction

G protein-coupled receptors (GPCRs) are the largest and most diverse group of membrane proteins which transmit extracellular stimuli into the cell interior of eukaryotes. It is canonically envisioned that a GPCR, upon activation by an external signal, couples to a G protein on the inner surface of membrane; the event leads to activation of the latter and consequent triggering of a sequence of downstream signaling pathways within the cell. Receptor desensitization usually occurs when it becomes phosphorylated by a GPCR kinase which shifts the sensitivity of the intracellular coupling interface to prefer arrestin proteins [1, 2]. More recent research, however, indicates tremendously complex signaling patterns for many GPCRs; the receptor may couple to more than one type of G protein triggering a plethora of alternative intracellular pathways; arrestin recruitment induces additional, G-protein independent signaling that affects the cell function [3]. All these concerted

cellular actions can be fine-tuned by a ligand molecule bound to the extracellular binding domain and a very important observation in current GPCR pharmacology is biased agonism [4]. It occurs when structurally different ligands, upon binding to the same receptor, trigger significantly altered cellular signaling by inducing unequal interaction patterns between a receptor and intracellular transducers (G proteins and/or arrestins) [5–8]. While pharmacologic aspects of biased agonism becomes well documented and described for growing number of GPCRs, its structural basis and key drug–receptor interactions directing receptors for biased signaling remains much more elusive [9].

β_2-adrenergic receptor (β_2-AR) is one of the best-characterized GPCRs from both pharmacologic and structural standpoints [10]. Plenty of β_2-AR ligands, agonists, antagonists, or inverse agonists have been developed [11] and many of them are in clinical practice [12, 13]. Research suggests that some of the ligands show biased patterns of signaling [14]. For example, when analyzing the cellular ratio between cAMP response (associated with the receptor's Gs coupling) and GRK response (mediated by β-arrestin recruitment) for a series of β2-AR agonists, three outliers were identified that showed a significant bias toward arrestin signaling: N-cyclopentylbutalephrine, isoetharine, and ethyl-norepinephrine [15]. Another study on rat cardiomyocytes [16] indicated that activation of β_2-AR by a standard agonist leads the receptor to couple to G_s and, to a lesser extend to G_i protein; the exemption was observed for fenoterol, an agonist which induced solely G_s signaling patterns in the experimental setup. In the follow-up study, different stereoisomers of fenoterol and its derivative, 4-methoxyfenoterol were analyzed; it was found that in both structures, the (R,R) stereoisomers induced G_s selective signaling patterns, while (R,S) isomers showed dual signaling, G_s plus significant component of G_i [17].

β_2-AR is also the first druggable GPCR, which x-ray crystallography structure was determined as early as in 2007 [18]. Since then, numerous groups have been resolving structures of the receptor complexed with varied ligand molecules within the binding site and transducers or nanobodies bounded to the intracellular coupling interface of the receptor in its active forms [19–22]. Numerous lines of evidence postulate the allosteric coupling mechanism of β2-AR and other representatives of class A GPCRs. The receptor can be envisioned as a shapeshifting molecule, where the binding of a ligand in the extracellular binding pocket induces an outward movement of the receptor's helices, which leads to adopting a shape compatible with the binding of a given transducer. Given that such a three-component system (ligand + receptor + transducer) remains in a state of dynamic equilibrium, the binding of the transducer in the intracellular part can affect the shape of the ligand binding pocket located there [23, 24]. This effect has significant implications for ligand-directed signaling; different ligands constrain the receptor to slightly different active conformations, which may result in unequal transducer interactions with the intracellular binding interface. Additionally, transducer binding may also affect ligand binding and modulate drug affinity. Therefore, the allosteric mechanism may link a specific transducer to a preferred (or biased) ligand and vice versa. Another important observation is that the ligand binding pocket at adrenergic receptors can be subdivided into two sectors: the orthosteric site, where (nor)epinephrine binds and the extended ligand binding domain (ELBD) [8]. The latter accommodates the fraction of an exogenous agonist molecule beyond epinephrine pharmacophore and is less evolutionary conserved than the ortosteric site, thus utilized by medicinal chemists for the development of subtype-selective ligands. But more importantly, residues composing ELBD originate from the external tips of transmembrane helices and the extracellular loop 2 (ECL2) cap, the region considered as the most important to perform the allosteric link between a biased agonist and preferred transducer [8]. This is suggested by an analysis based on the molecular structure of ligands [25], showing that arrestin-biased agonists [26–28] have an aryl-substituted alkyl tail attached to the amino N atom, and the bulky aromatic rings that occupy the ELBD [20, 21, 29]. In contrast, the Gs-biased agonists also occupy this space but form distinct interactions [30]. The interaction of biased agonists with the ELBD is also observed in molecular simulations [31, 32].

In extensive research on the mechanism of action of the β_2-AR receptor, methods based on molecular simulations play a significant role, enabling insight into the details of interactions responsible for specific conformational states and attempting to link the stability of particular conformers with the effect of the presence of a given pharmacological type of ligand. In recent years, atomistic-level simulations have allowed, among other things, the determination of molecular details of the β_2-AR receptor activation mechanism [33–35], as well as analogous details, for instance, for receptors with mutations [36] and/or biased signaling processes [31, 32, 37].

The current work relies on a molecular modeling approach to corroborate the allosteric coupling mechanism. The main aim is to investigate ligand-induced structural changes of the β_2-AR molecule that link a biased molecule in the binding site with structural organization of the intracellular interface recognizing a transducer using atomistic molecular dynamics (MD) simulations carried out according to either standard, unbiased, or enhanced-sampling (metadynamics-based) protocols. The study is focused on modeling of two the most active stereoisomers of 4′-methoxy-1-naphtylfenoterol (MNFen), that is, (R,R)- and (R,S)-; it was earlier determined that stereochemistry of that ligand significantly affects interactions with β_2-AR and is a source of biased signaling observed in β_2-AR-$G_s\alpha$ and β_2-AR-$G_i\alpha$ fusion proteins [38, 39]. In light of the results obtained from the atomistic simulations, additional coarse-grained (CG) simulations were conducted to verify the reproducibility of the most significant observations.

It is worth emphasizing that the two studied ligand-GPCR complexes differ only by stereoconfiguration of the ligands bound to receptor. Apart from this factor, all other details of the applied molecular model (including the Hamiltonian describing intra- and intermolecular interactions, system composition, etc.,) are identical. This creates a unique opportunity to investigate the fundamentals of biased agonism while simultaneously minimizing the effects related to structural differences in ligands that are not stereoisomers, which could influence the obtained results. Such effects may be associated, for example, with the accuracy of the model but also with the variable time scale of the

observed processes. Therefore, any found and discussed differences between the dynamic structure of the complexes induced by the presence of the ligand have their source only in the type of ligand stereoconfiguration.

2 | Methods

2.1 | Docking

The docking study and MD simulations involving β_2-AR relied on the XRD structural data deposited in the PDB database (PDB:4LDL). The T4 lysozyme, present alongside β_2-AR, as well as all cocrystalized small molecules and ions were removed from the receptor structure. Subsequently, the docking simulations were carried out in order to find the most energetically favorable initial positions of the two stereoisomers of MNFen in the binding cavity of β_2-AR.

The considered ligand molecules, (R,R)-methoxynaphtylfenoterol ((R,R)-MNFen), (R,S)-methoxynaphtylfenoterol ((R,S)-MNFen) and hydroxybenzylisoproterenol (i.e., ligand originally present in the PDB:4LDL structure) were drawn using Avogadro 1.1.1 [40], relying on the hydroxybenzylisoproterenol structure and initially optimized within the UFF force field [41] (5000 steps, steepest descent algorithm). These flexible and optimized ligands molecules were docked into the binding pocket of the receptor, prepared as described above. Docking simulations were carried out in the AutoDock Vina software [42, 43]. The procedure was performed within the cuboid region of dimensions of $24\times24\times24$ Å^3 which covers all the originally cocrystallized ligand present in the considered PDB structure as well as the closest amino-acid residues that exhibit contact with that ligand. All default procedures and algorithms implemented in AutoDock Vina were applied. The torsional angles in ligand molecules as well as the selected amino-acid sidechains within the binding cavity were allowed to rotate. For each ligand, a single docking was performed, resulting in the generation of 8 alternative ligand locations along with their corresponding binding energies. The criterion for classifying a given ligand position as "favorable" was the binding free energy determined during docking. Moreover, the inspection of the poses obtained during docking was carried out, along with clustering analysis. The most favorable binding poses of (R,R)-MNFen and (R,S)-MNFen interacting with β_2-AR were accepted as starting configurations in the subsequent MD simulations. The hydroxybenzylisoproterenol-containing system was not considered in the context of MD simulations, and its role was only to validate the docking protocol.

2.2 | Atomistic MD Simulations

The MD simulations relied on the PDB:4LDL structure. The β_2-AR-ligand complexes of the structure determined during docking simulations were placed in rectangular simulation boxes of dimensions $12\times12\times14$ nm^3, immersed in the DPPC lipid bilayer, and surrounded by the explicit water molecules (ca. 40 000) and appropriate number of Na^+ and Cl^- ions (ca. 160), neutralizing the charge and elevating the ionic strength to 0.15 M. GROMACS 2016.4 [44] tools were used for this purpose, including pdb2gmx, editconf, solvate, and genion subprograms. The systems were subjected to a multistep geometry optimization and equilibration protocol relying on gradual removing constraints from the protein structure in parallel to applying the pressure control. The following steps were applied: (1) frozen protein, positional restraints with force constants equal to 1000 kJ/mol/nm^2 on heavy atoms of lipids, 1 ns NVT simulation; (2) positional restraints with force constants equal to 1000 kJ/mol/nm^2 on each heavy atom of protein, 5 ns NPT simulation; (3) positional restraints with force constants equal to 100 kJ/mol/nm^2 on protein backbone, 5 ns NPT simulation; (4) positional restraints with force constants equal to 10 kJ/mol/nm^2 on protein backbone, 5 ns NPT simulation; (5) unconstrained NPT simulation lasting 15 ns. After equilibration, systems were subjected to the standard, unbiased MD simulations or the free energy calculations (see details below).

All MD simulations, including stages of geometry optimization and equilibration, were carried out within the GROMACS 2016.4 package [44] by using the all-atom CHARMM36 force field [45]. The parameters for ligands were generated by the CHARMM-GUI online server [46] whereas the GROMACS build-in pdb2gmx tool was used for generating protein-related parameters. Periodic boundary conditions and the isothermal-isobaric ensemble were applied. The temperature was maintained close to its reference value (310 K) by applying the V-rescale thermostat [47], whereas for the constant pressure (1 bar, semiisotropic coordinate scaling), the Parrinello-Rahman barostat [48] was used with a relaxation time of 0.4 ps. The equations of motion were integrated with a time step of 2 fs using the leap-frog scheme [49]. The TIP3P model of water [50] was applied. The hydrogen-containing solute bond lengths were constrained by the application of the LINCS procedure with a relative geometric tolerance of 10^{-4} [51]. The electrostatic interactions were modeled by using the particle-mesh Ewald method [52] with cutoff set to 1.2 nm, while van der Waals interactions (LJ potentials) were switched off between 1.0 and 1.2 nm. The translational center-of-mass motion was removed every timestep separately for the solute and the solvent. The full rigidity of the water molecules was enforced by the application of the SETTLE procedure [53]. Production simulations were carried out for a duration of 1000 ns, and the data were collected every 2 ps.

The analysis of RMSD (root-mean square deviation) was performed by using the gmx rms tool (part of GROMACS) and concerned C_α atoms of selected parts of the β_2-AR structure. The distance between fragments of transmembrane domains was always calculated as the center-of-mass of three consecutive C_α atoms, located on the α-helix and being closest to the nearest loop (or N-end).

The free energy calculations were carried out according to the well-tempered metadynamics protocol [54] by using PLUMED 2.4 software [55]. The equilibrated configurations of both considered systems were used to initiate the metadynamics simulations. The 1D free energy profiles (FEPs) were defined by the value of the N-C_1-C_2-C_3 dihedral angle (see the illustration and atom numbering in Figure 3), which expresses the orientation of one of the ligand moieties. The parameters of metadynamics were set as follows: initial height of bias portion: 0.2 kJ/mol, bias portion width: 0.314 rad, initial deposition rate: 1.25 kJ/mol/ps, bias factor (dependent on the ΔT parameter in Eq. (2)

from ref. ([54]: 15). Metadynamics simulations were carried out for 200 ns, and the convergence of the final FEPs was tested by hand-written scripts.

Additionally, to estimate the free energy of binding of both MNFen stereoisomers to the receptor, two 100 ns simulations of the free ligands in the solvent were carried out. The remaining simulation parameters were kept the same (except for the size of the simulation boxes, which were reduced to $6\times6\times6\,nm^3$).

2.3 | Coarse-Grained MD Simulations

The initial protein structure for CG simulations was the same as that for atomistic simulations (i.e., PDB:4LDL). It was converted to CG resolution by using the martinize2.py script; the same script was used to generate the initial force field parameters. The missing ICL3 fragment was reconstructed by using the MoMA-LoopSampler online server [56] (moma.laas.fr). The Martini 3 [57] parameters were employed in the simulations. Instead of the default elastic network approach, the GōMartini [58, 59] protocol was applied to restrain the secondary and tertiary protein structure with default options, including dissociation energy of the Lennard-Jones potentials equal to 12 kJ/mol. The create_go-Virt.py script was applied for that purpose. Moreover, the depths of the GōMartini energy terms linking TM1 with TM7 and TM1 with TM2 were reduced to 9.0 kJ/mol, and the GōMartini potentials associated with loops were removed in order to better reflect the disordered nature of these fragments.

The presence of ligand molecules was not explicitly considered in the CG model. In order to reflect the conformation of the receptor characteristic of the given stereoisomer of MNFen, a series of restraints was applied on the selected molecular switches, namely: (1) the distance between sidechains of Lys305 and Asp192 (< 0.6 nm for (R,S)-MNFen-like conformer and > 0.9 nm for (R,R)-MNFen-like conformer); (2) The BB_{Asn}-BB-SC_1-SC_4 torsional angle controlling the orientation of the Trp313 sidechain (−55 or 165 deg., respectively, according to the Martini3 notation); (3) The BB-SC_1-SC_4 angle, keeping the realistic orientation of the Trp313 sidechain with respect to TM7 and TM1 (100°, for both systems); (4) the three types of distance restraints between sidechain atoms of Trp313 and backbone atoms of Ile309, Ala91, and Val87 aimed to force the Trp313 orientation known from atomistic MD simulations. Other criteria for the choice of restraint-related parameters also relied on the results of atomistic simulations. The CG simulations were focused on two separate systems, differing only by configuration of the above-mentioned switches.

Initially, the β_2-AR molecule was placed in rectangular simulation box of dimensions and $14\times14\times21\,nm^3$. The immersion of β_2-AR into lipid bilayer and the subsequent solvation in the Martini 3 water was carried out by the insane.py script. The lipid bilayer included: POPC (molar fraction: 18%), POPE (21%), POPS (11%), cholesterol (34%), and palmitoylsphingomyelin (16%).

All CG MD simulations were carried out with the GROMACS 2023.2 package [44]. The reaction field electrostatics and Lennard-Jones potentials were shifted to zero at the cutoff distance of 1.1 nm. A dielectric constant of 15 was employed up to the cutoff length, after which it was given a value of infinity. The Verlet cutoff scheme was employed, as implemented in GROMACS. Temperatures of the protein, the lipids and the solvent were separately kept constant at 310 K in accordance with the procedure described in the previous section. After geometry optimization and equilibration (lasting 100 ns), the CG production simulations for both systems were carried out for a duration of 10 μs, and the data were saved every 20 ps. The restraints distinguishing between two systems were turned on at the stage of equilibration.

The distances between intracellular fragments of transmembrane domains were defined as in atomistic simulations.

3 | Results and Discussion

3.1 | Docking Results

In the case of all ligands, it was noted that the most favorable interaction energies (2 or 3, depending on the system under consideration) corresponded only to minimal conformational changes of the ligand, related to rotations in the hydroxyl groups, while the ligand's position relative to the protein remained the same. Second and third highest energies (higher from the most favorable one by at least 4.6 kJ/mol) corresponded to rotations of one of the groups containing naphtyl rings in MNFen, while the ligand's position relative to the protein remained unchanged. Only notably highers energies (at least 6.7 kJ/mol above the lowest) corresponded to significant changes in the structure of the complexes. When considering the lowest energy and the pose associated with it, the applied docking methodology appeared to be accurate enough to recover the position of the hydroxybenzylisoproterenol, known due to the XRD structure (PDB:4LDL) (Figure 1A). Initial positions of methoxynaphtylfenoterol stereoisomers interacting with the binding cavity of β_2-AR appeared to be highly similar to the structurally related hydroxybenzylisoproterenol, present in the binding cavity of the XRD structure of PDB:4LDL (Figure 1B). This is expected in view of highly similar structures of both hydroxybenzylisoproterenol and methoxynaphtylfenoterol molecules. Moreover, binding of (R,R)-MNFen is slightly more energetically favorable in comparison to (R,S)-MNFen (−46.9 vs. −46.0 kJ/mol) which is in line with existing reports, indicating the enhanced affinity of (R,R)-stereoisomers of fenoterol derivatives with respect to binding to β_2-AR over alternative stereoisomers [60].

3.2 | Interactions of Ligands With Binding Cavity

The results in this and the following sections 3.2–3.4 are based on atomistic MD simulations, carried out according to the protocol described in section 2.2.

All ligands display stable position in the binding cavity of receptor during whole course of unbiased MD simulation (1 μs). The network of ligand–receptor interactions found in the XRD structure (PDB:4LDL) and concerning the structurally analogous ligand (hydroxybenzyl isoproterenol) is fairly well recovered also in the case of the two MNFen-β_2-AR complexes. This includes for example, the ionic bridge between Asp113 and amine moiety

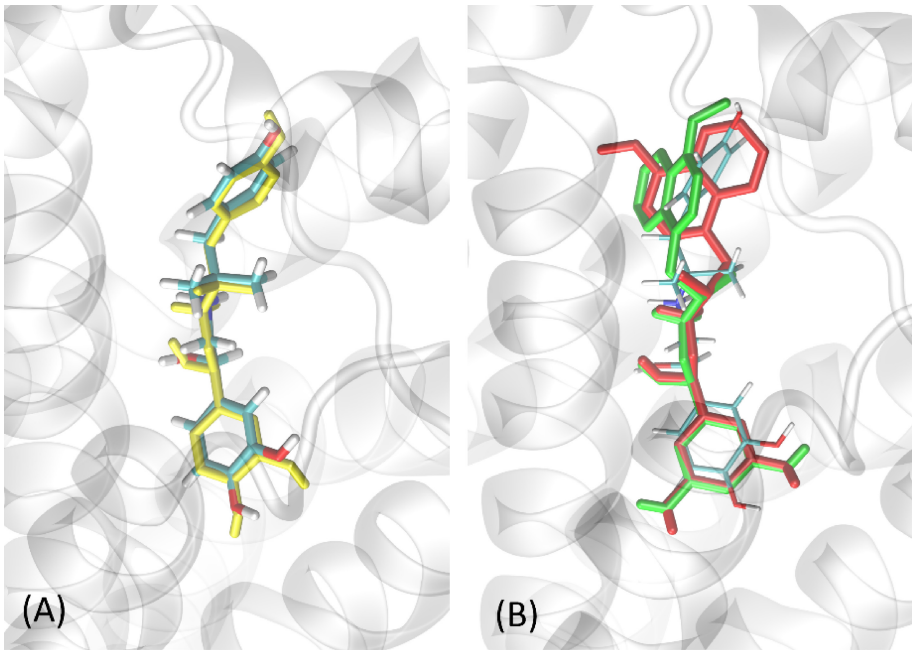

FIGURE 1 | The graphical illustration of the docking results. (A) Superposition of the crystal structure of the hydroxybenzylisoproterenol molecule (PDB:4LDL, colored in yellow) and the optimal structure of the same ligand recovered during docking study (colored by atom type). (B) Superposition of the most energetically favorable ligand arrangements found during docking study for hydroxybenzylisoproterenol (colored by atom type) and the two stereoisomers of MNFen: (R,R) (colored in green) and (R,S) (colored in red).

of ligand, which is one of the most frequently conserved contacts in the ligand-β_2-AR interactions. Both (R,R)- and (R,S)-MNFen molecules occupy the same binding region between transmembrane domains (TM): TM3, TM5, TM6, and TM7. Other relevant protein–ligand contacts include: (1) the two meta-OH groups of the 3,5-dihydroxyphenyl moiety of ligands create hydrogen bonding (HB) with Ser203 and Ser207 located on TM5, (2) β-OH moiety of the ligand can form HB involving Asp113 (TM3) and Asn312 (TM7), (3) amine moiety of ligand can interact with Asn312 by creation HB, and (4) the 4-methoxynaphtyl moiety (MeO-Naph) of the ligand is located in the vicinity of TM7. It is also worth noting the close distance between the ligand molecule and Trp286, that is, the residue that was identified in our previous studies as a potential conformational switch playing a role in stabilizing certain conformational states of the receptor. Figure 2A,B illustrates the location of both ligands in the binding cavity and shows all amino-acid residues located in the vicinity of the ligand molecules.

Using the linear interaction energy method [61], the free binding energy of both stereoisoforms of MNFen to the receptor was estimated. Values of −26.4 and 25.2 kJ/mol were obtained for (R,R)-MNFen and (R,S)-MNFen, respectively, which is in agreement with the affinity trend obtained in docking ((R,R) > (R,S)) and highlights the significant affinity of both ligands for the receptor.

During the whole runtime of the simulations (1000 ns) of MD simulation, the position of (R,R)-MNFen is roughly unchanged with respect to the initial arrangement (Figure 1) which includes the direction of the 4-MeO-Naph of the ligand toward Tyr308. On the contrary, the fragment of (R,S)-MNFen undergoes a reorientation after ca. 240 ns of simulation. Namely, the 4-MeO-Naph rotates and approaches amino-acid residues located at TM1, TM2, and ECL2. The position of the remaining parts of ligand molecules is unaltered with respect to the initial structure. This effect is clearly seen in Figure 2C, where these regions of the receptor display quantitative differences in the contact pattern and/or intensity with the ligand molecule, depending on ligand's stereoconfiguration. In more detail, the alteration in the network of the ligand–receptor interactions includes the new contacts with for example, Gly90 and Ala91 (TM2), more intensive contacts with His93 (TM2) and, in general, significant reduction of the distance to TM1. On the other hand, a series of contacts with residues on ELC3 are reduced with respect to their intensity. This includes mainly residues 300–308, including Lys305 and Tyr308, as mentioned in further paragraphs. Moreover, although the corresponding average distance is roughly unchanged, the geometry of the arrangement of the 4-methoxynaphtyl group maintaining contact with Trp109 is disturbed, which certainly influences the strength of the associated π-π or CH-π interactions with Trp109 (TM3), Ile309, Trp313 (TM7), and Phe193 (ECL2). The discussed reorientation of ligand's moiety has a character of a so-called rare event [62]; that is, it is nearly instantaneous (needs only tens of ps to be completed) and is irreversible when considering the remaining simulation time. Figure 3A,B shows further molecular details of the discussed transition, including their influence on the rotameric states of Trp313 and Met40 sidechains as well as on the Lys305-Asp192 ionic bridge. This will be discussed further in section 3.3.

The timescale characteristic of the above-mentioned structural rearrangement (hundreds of ns) is too large to estimate the related conformational equilibria by using the unbiased MD simulations. Therefore, the enhanced-sampling, metadynamics-based protocol was applied to determine the relative favorability of the 4-MeO-Naph. The results confirm that the reoriented

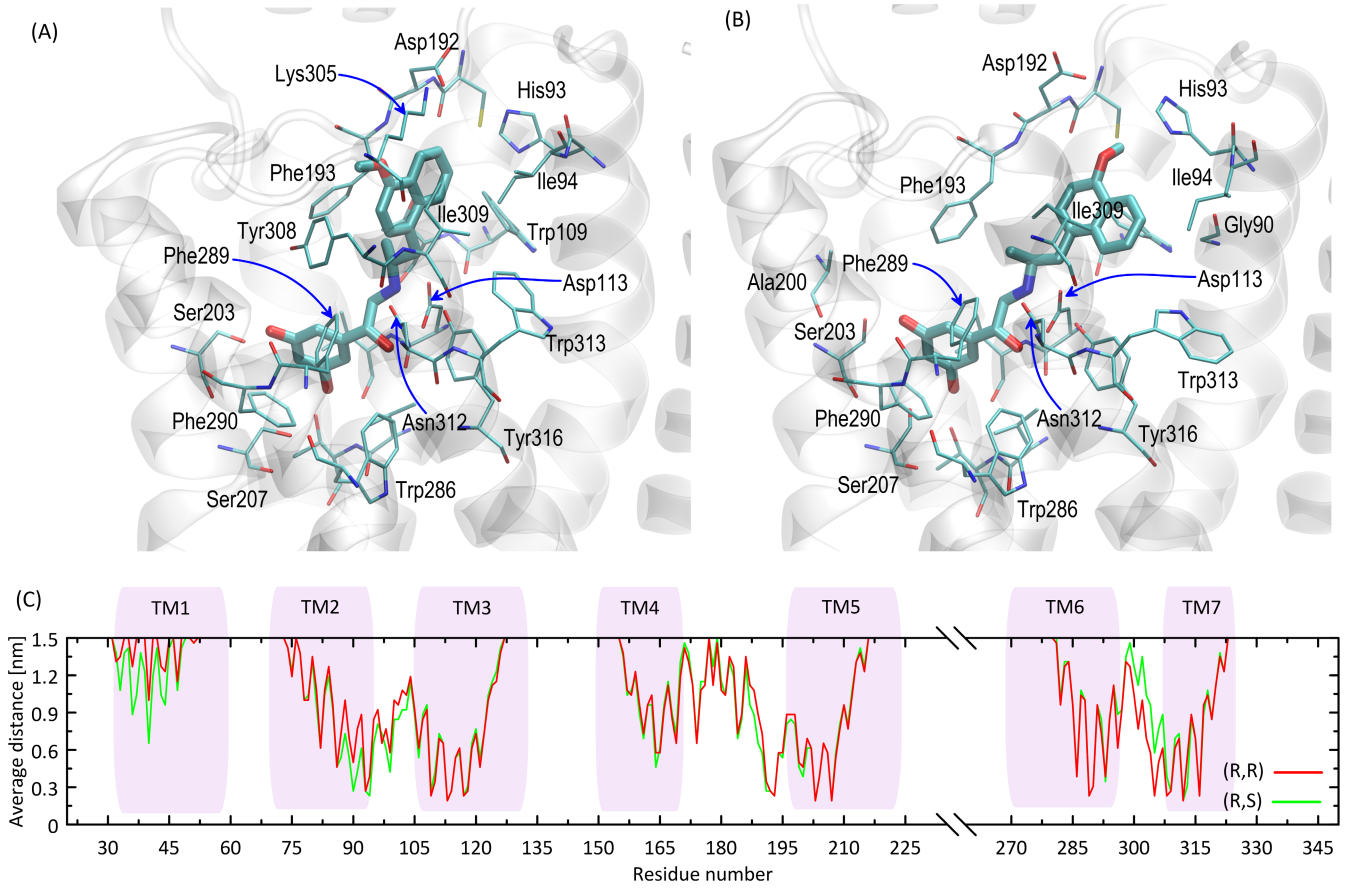

FIGURE 2 | (A) Typical position of the (R,R)-MNFen molecule in the binding cavity of the receptor, identified based on atomistic MD simulations. The ligand molecule is shown using a thick stick representation, while the nearest amino acid residues in contact with it (distance less than 0.4 nm) are shown as thin sticks. Hydrogen atoms are omitted for clarity. The illustration is based on the final frame of the unbiased MD simulation. (B) As in (A), but the ligand is (R,S)-MNFen. (C) The average minimum distance between the ligand molecule and all amino acid residues in the β_2-AR molecule.

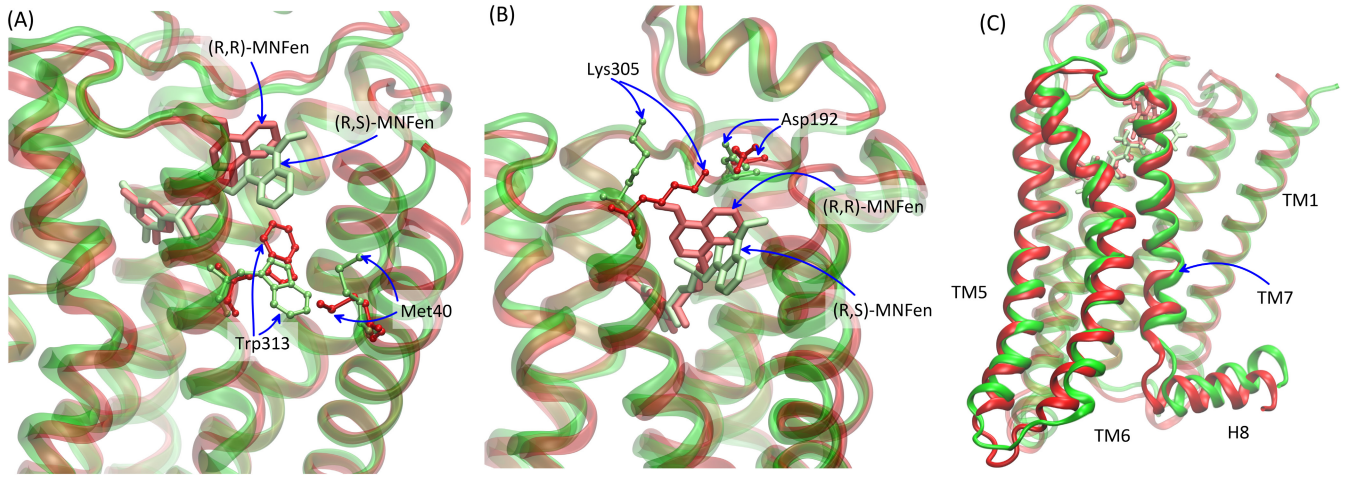

FIGURE 3 | (A) The position of the (R,S)-4-methoxynaphtylfenoterol molecule (colored in green) bound to β_2-AR compared to the position of (R,R)-4-methoxynaphtylfenoterol (colored in red) and the reorientation within the Trp313 and Met40 sidechains, correlated with the ligand stereoconfiguration. The color code is uniform for all panels. (B) Same as in (A) but with the two conformations of the Lys305-Asp192 ionic bridge, also correlated with the stereoconfiguration of bound ligand. (C) The structural changes in the β_2-AR molecule, visible especially the intracellular part of the β_2-AR, correlated with the stereoconfiguration of the ligand present in the binding cavity.

group of (R,S)-MNFen corresponds to the most energetically favorable conformation. Moreover, the undisturbed arrangement of the (R,R)-MNFen molecule is also the most favorable conformation typical for this ligand. The energy levels for alternative conformers exceed 20 kJ/mol in both cases; thus, their presence can be safely neglected. The 1D FEPs characteristic of the rotations of the MeO-Naph group are given in Figure 4. Apart from the initial fragments of MD trajectory generated for (R,S)-MNFen

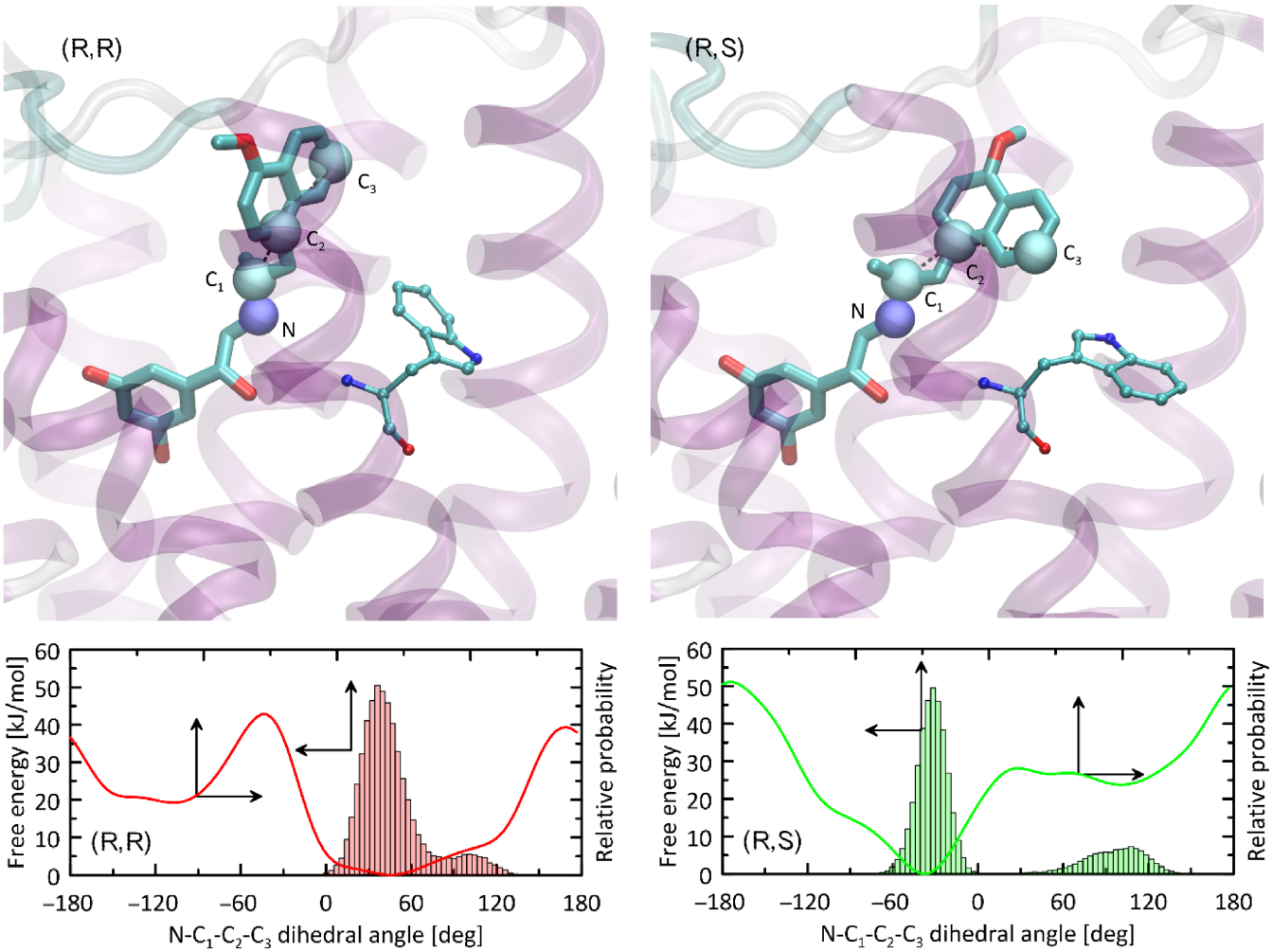

FIGURE 4 | (up) The definition of the metadynamics coordinate, that is, the N-C_1-C_2-C_3 dihedral angle (atoms defining the quadruplet are marked as balls) and the orientation of the Trp313 sidechain, correlated with the ligand stereoconfiguration. (down) The 1D free energy profiles were calculated during 200 ns-long metadynamics simulations (solid lines), and the histogrammed values of the N-C_1-C_2-C_3 dihedral angle were sampled during unbiased 1 μs-long MD simulations.

(ca. 24%), the sampled conformational space and related quantities discussed below correspond to energetically favorable orientations determined in this stage of the study.

A direct consequence of diverse arrangements of both stereoisomers in the binding cavity is a series of differences between particular structural descriptors reflecting for example, the distances between reoriented MeO-Naph group (as discussed earlier) but also some of amino acid residues present in the binding pocket. In the next subsection, the "local" structural changes occurring within the binding cavity or its close vicinity are described and discussed; the changes taking place in more distant parts of the receptor, especially those observed in the intracellular parts are concerned in subsection 3.4.

3.3 | Structural Consequences for Extracellular Part of β_2-AR

Only very few amino-acid residues differ in their conformation upon the influence of a reoriented MeO-Naph group of (R,S)-MNFen in comparison to the case of (R,R)-MNFen. The most essential differences include the sidechains of His93, Ile94 (TM2), Trp313 (TM7), and Met40 (TM1). The "twisted" MeO-Naph group of (R,S)-MNFen creates the sterically-crowded environment in the vicinity of TM2 and TM7, forcing the systematic movement of the His93 and Ile94 sidechains further from the binding cavity. The same effect is responsible for the orientation of the Trp313 sidechain which is faced toward TM1. Consequently, the Met40 sidechain is reoriented in order to accommodate the indole moiety of Trp313, now maintaining closer contact with TM1. On the contrary, in the case of (R,R)-MNFen, the analogous MeO-Naph group is placed closer to TM6, leaving the space to accommodate the rotating Trp313 sidechain and slight movement of His93 and Ile94 toward the centre of the binding cavity. Thus, the most significant, well-defined ligand-induced alteration in the conformation of binding cavity are the distinct rotameric states of Trp313 (see Figures 3A,B and 5A). The conformation of Tyr308, that is, the residue which has been identified as relevant for the biased-agonism phenomena [63], is roughly the same in the case of both considered ligands. However, the stereoconfiguration-inherent structural differences result in a lack of any contact between the MeO-Naph group

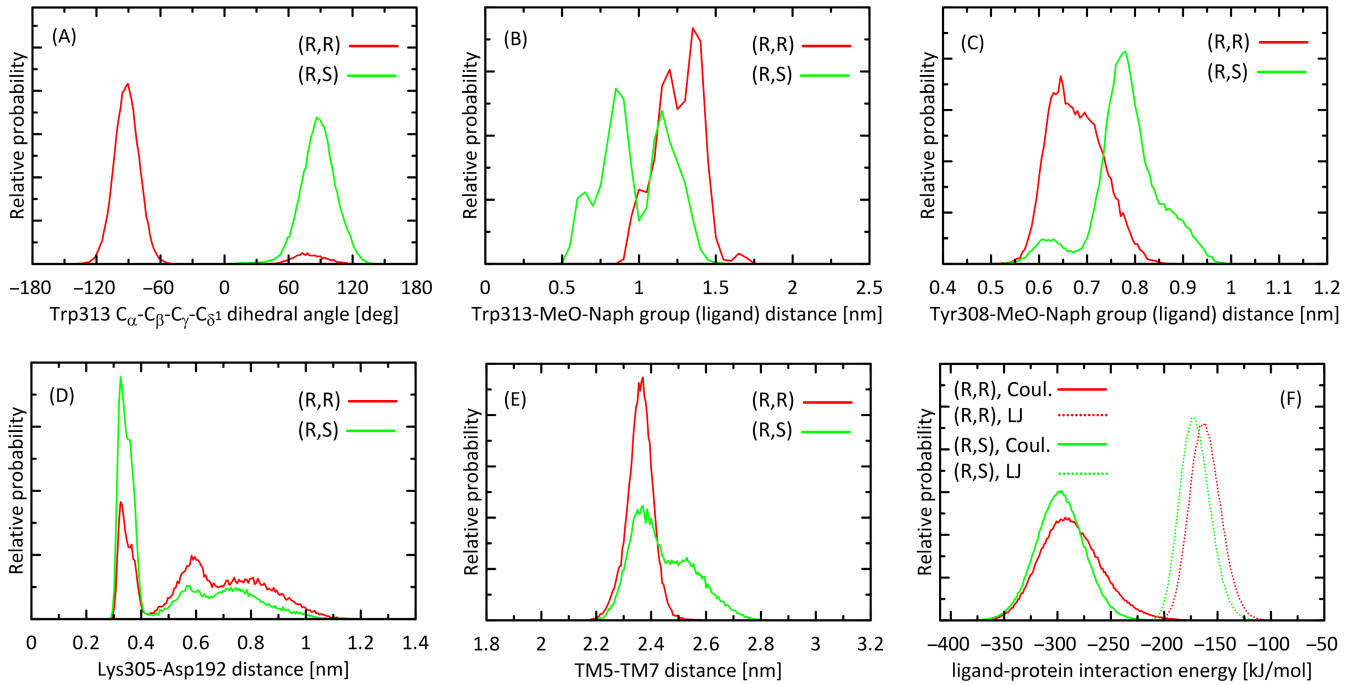

FIGURE 5 | A series of probability distributions related to the selected descriptors illustrating either the ligand-affected conformation of β_2-AR (A, D, E), the ligand–protein contacts (B, C) or the ligand–protein energy of interactions (F). The distances were measured either for COM of sidechains and the MeO-Naph group (B, C, D) or selected C_α atoms, corresponding to intracellular fragments of the domains (E).

of (R,R)-MNFen and Tyr308 sidechain. On the contrary, such contacts are frequently maintained in the case of (R,S)-MNFen (Figure 5B). In general, the network of interactions within the receptor, under the influence of the (R,S)-MNFen molecule in the binding pocket, shifts toward stronger steric pressure exerted by the side chain of Trp313 and the ligand itself on TM1 and TM2.

Interestingly, the available XRD structures of the β_2-AR-agonist complexes usually contain only one type of the Trp313 rotamer, compatible with that identified in our simulations of (R,S)-MNFen-containing system. A more detailed discussion on the conformations of Trp313 in the XDR structures is given in section 3.6.

Moreover, we have observed a notable alteration of the dynamic equilibrium inherent to opening/closing of the Lys305-Asp192 ionic bridge (Figures 3A,B and 5D). The presence of (R,S)-MNFen in the binding cavity shifts this equilibrium toward the preference of the closed state and direct contact of the involved sidechains. This results from the stabilizing influence of the methoxy group of the (R,S)-MNFen molecule interacting with Asp192. On the contrary, the analogous group of (R,R)-MNFen is capable to interact with the sidechain of Lys305, competing for interactions with Asp195 and, thus, reducing the chances for ionic bridge formation.

Depending on the residue considered, the mentioned conformational rearrangements within the protein molecule are either rare-event transitions, irreversible within the simulation timescale, and correlate with the reorientation of the (R,S)-MNFen group. The main example belonging to the first group is the reorientation of the Trp313 sidechain, which occurs at the beginning of the simulations, and no further changes are observed until the end of the run. Other transitions are of a dynamic nature, and the reorientation of the ligand group shifts their dynamic equilibrium. In this case, the examples are are follows: (1) the most frequently occurring conformation (ca. 70% in both cases) of the His93 sidechain, which can correspond to the C_α-C_β-C_γ-$C_{\delta1}$ torsional angle values of ca. −170° (for (R,R)-MNFen) or ca. −90° (for (R,S)-MNFen); (2) the conformation of the Ile94 sidechain, which can correspond to three nearly equally populated staggered conformers around −60°, 60°, and 180° (for (R,R)-MNFen) or to a single, dominating conformer with a frequency of ca. 80% at ca. 170° (for (R,S)-MNFen) (the C-C_α-C_β-C_γ torsional angle was considered); (3) the population-dominating conformation of the Met40 sidechain, which is increased from ca. 50% to 65% upon changing the ligand type from (R,R)-MNFen to (R,S)-MNFen (the C-C_α-C_β-C_γ torsional angle is equal to ca. 180° in both cases); (4) the frequency of appearance of the Lys305-Asp192 ionic bridge, which is equal to either 26% ((R,R)-MNFen) or 66% ((R,S)-MNFen).

3.4 | Structural Consequences for Intracellular Part of β_2-AR

The pattern of ligand–protein contacts observed for considered stereoisomers of MNFen is correlated with a series of structural divergences of the receptor molecule considered at a larger dimensional scale. More precisely, the observed differences are located in the intracellular part of β_2-AR and include moderate structure reorganizations at the interface of TM7/H8 (8th helix) and TM5/6. The superposition of the resulting receptor structure is shown in Figure 3C, and the distribution of the exemplary descriptor (distance between intracellular fragments of TM5 and TM7) is given in Figure 5E whereas Figures 6 and 7 show the results of a more systematic analysis oriented

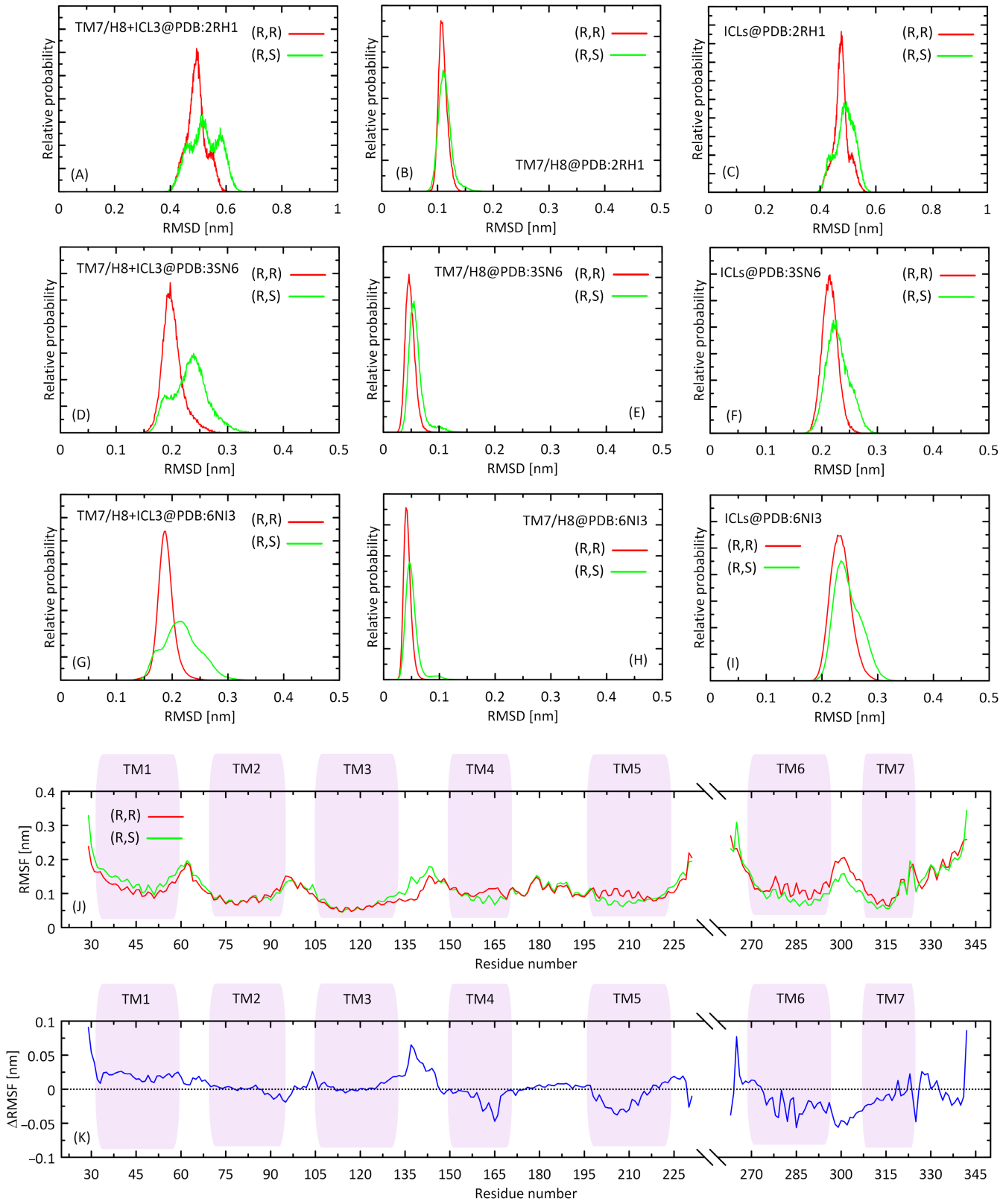

FIGURE 6 | (A–I) The distributions of the RMSD values calculated for intracellular parts of the receptor (either ICLs or TM) with respect to the three different crystal structures of β_2-AR: PDB:2RH1 ('inactive' conformer of β_2-AR), PDB:3SN6 ('active', Gs-coupled β_2-AR) and PDB:6NI3 (β_2-AR bound to β-arrestin). (J) The RMSF values were calculated for all C_α carbon atoms within the β_2-AR-ligand complex. The PDB:3SN6 structure was used as a reference for calculating RMSF. (K) Difference between RMSFs is shown in panel (J).

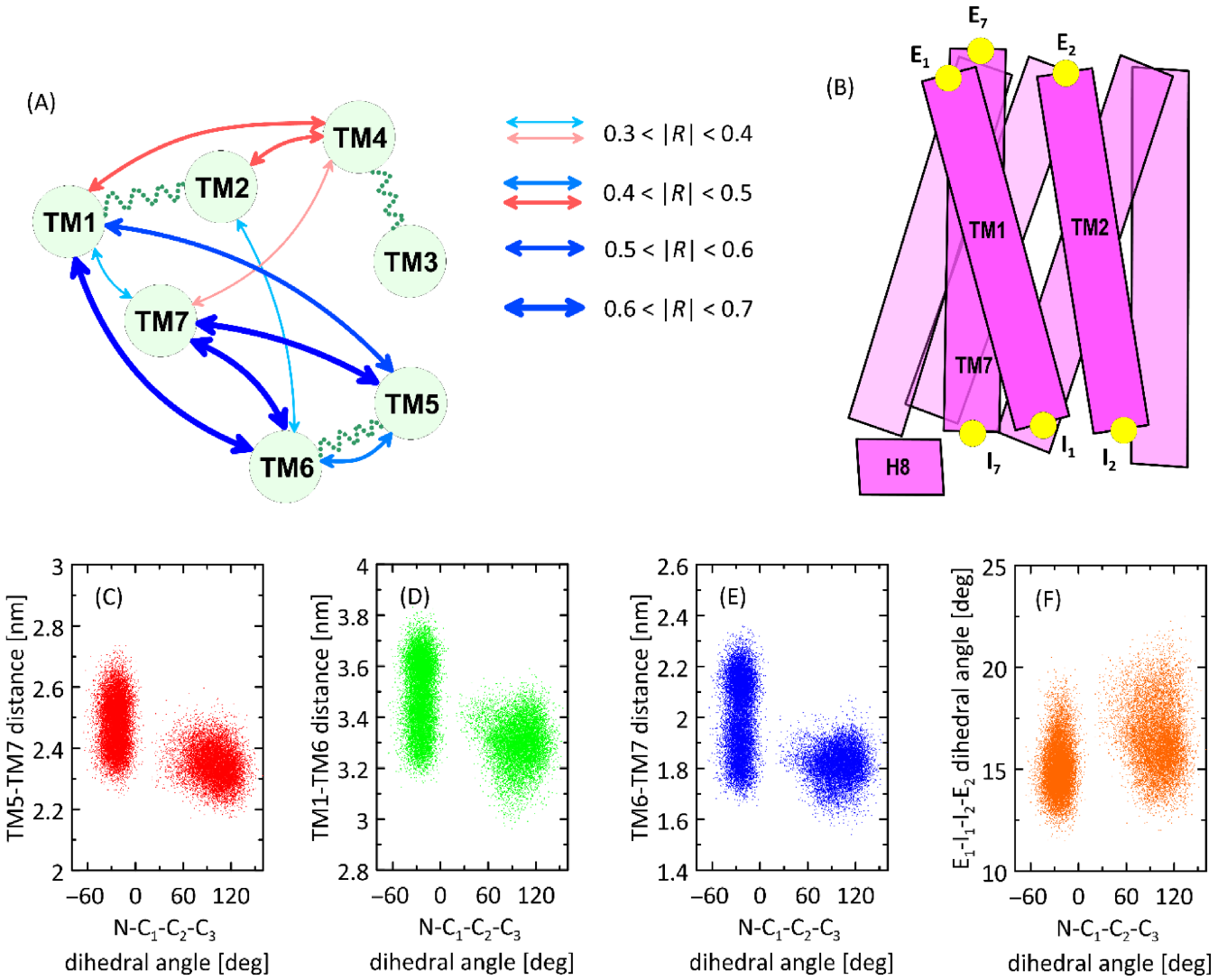

FIGURE 7 | (A) Symbolic illustration of the relationship between the distances of intracellular, terminal fragments of transmembrane domains caused by the conformational change of the (R,S)-MNFen ligand. The correlation coefficient (R) between the N-C_1-C_2-C_3 torsion angle (as shown in Figure 4) and the distances between these fragments was analyzed. All relationships corresponding to $|R| > 0.3$ are shown. Red arrows indicate a positive correlation (decreasing domain-domain distance), while blue ones indicate a negative correlation (increasing distance). (B) Symbolic illustration of the receptor, showing the definition of some of the analyzed fragments. (C–E) The three most strongly correlated descriptors. (F) The most strongly correlated descriptor among those representing the relative orientation of entire domains.

at comparison between the ligand-induced changes in the domain–domain distances.

The (R,S)-MNFen-bound β_2-AR displays a larger value of the TM1-TM6, TM5-TM7 and TM6-TM7 distances (measured only for the intracellular fragments of those domains) in comparison to (R,R)-MNFen-bound receptor (Figures 5 and 7). On the other hand, the distance between TM1 and TM4 as well as between TM2 and TM4 increases. At the same time, these pairs of helices are the most susceptible to dependence on the relative positioning influenced by the stereoconfiguration of the associated ligand. This effect is quantitatively presented in Figure 8, for both the all-atom simulations discussed in this section and the CG simulations discussed in the next section.

Although such ligand-induced alterations of the conformation would suggest the increased ability to bind the G_s protein due to an increase of the area of the potential binding region, a quantitative analysis based on RMSD parameters (Figure 6) speaks for a more complex scenario. Namely, when comparing the dynamic conformation of β_2-AR with the XRD reference structures, it appears that the (R,R)-MNFen-bound receptor is more structurally similar to G_s-coupled β_2-AR (PDB:3SN6) in comparison to the (R,S)-MNFen-containing complex. Moreover, β_2-AR in complex with (R,R)-MNFen is more conformationally-restricted, exhibiting only one main conformational state expressed either with respect to the RMSD values or TM7-TM5 interdomain distance. The (R,S)-MNFen-bound receptor display more conformational heterogeneity in the context of both the mobility of TM7 and relation to the fixed PDB:3SN6 structure. At the same time, its dynamic conformation is further from the G_s-coupled β_2-AR structure in comparison to the (R,R)-MNFen-bound receptor. Thus, in spite of larger interdomain distances observed for (R,S)-MNFen-β_2-AR

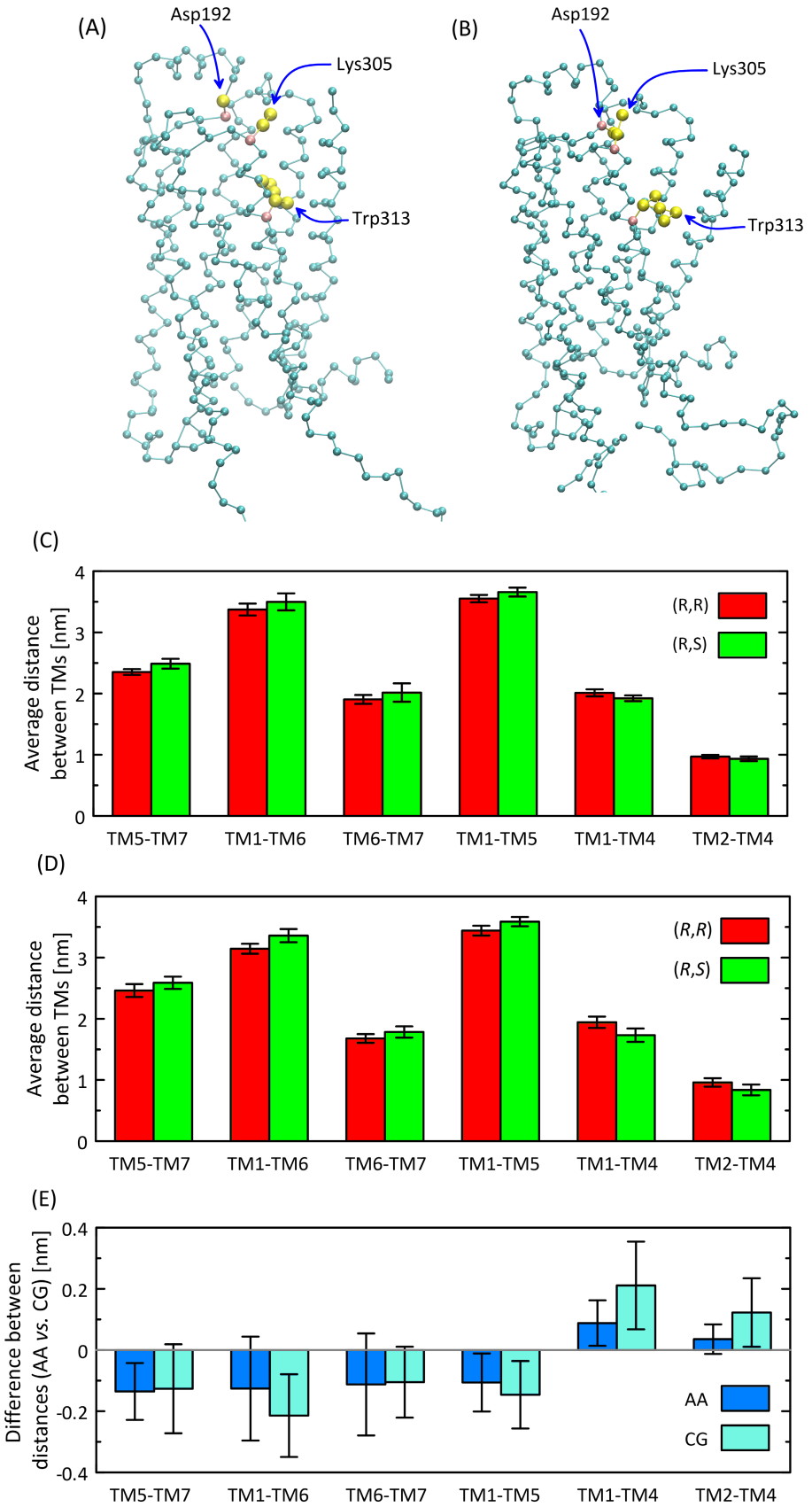

FIGURE 8 | (A and B) Symbolic representation of the coarse-grained models used in the simulations, along with different conformations of molecular switches, representing the receptor bound to (R,R)-MNFen (A) and (R,S)-MNFen (B). The interaction centers corresponding to the remaining sidechains have been omitted. (C) Average distance between the terminal intracellular fragments of the transmembrane domains determined using atomic simulations. (D) As in (C), but the data generated using coarse-grained simulations. (E) The difference between the values from panels (C and D) corresponding to different ligand stereoconfigurations according to simulations: Atomic (AA) and coarse-grained (CG).

complex, the (R,R)-MNFen-bound receptor seems to display a conformation that is more favored to G_s binding.

The above-described structural differences are restricted to the intracellular part of the receptor, mainly the interface between TM7/H8 and TM5/TM6 where both those regions are collectively accounted for in calculations of RMSD. The analogous parameters calculated within either sole TM5, TM6, TM7, or H8 reveal marginal differences between (R,S)-MNFen- and (R,S)-MNFen-bound receptors. The analogous calculations performed for all ICLs also indicate the same pattern of similarities between studies complexes and PDB:3SN6. This clearly indicates that the ligand-induced structural changes concern the conformational equilibrium between domains but not within single domains. The obvious exception here are the sidechain movements, related to the direct contact with the ligand molecules, described above.

Interestingly, in spite of structural alterations leading further from the PDB:3SN6 reference structure, the (R,S)-MNFen-β_2-AR does not become closer to the alternative, "inactive" antagonist-induced conformation of the receptor (Figure 5). In fact, both studied ligands induce conformations of the receptor that are nearly equally distant from the PDB:2RH1 one and much closer to the PDB:3SN6. Thus, in both cases, the sampled conformations can be classified as "active" ones but differ in a series of subtle structural details.

An analogous comparison was also made regarding the structure of the β_2-AR receptor bound to β-arrestin (PDB:6NI3), as shown in panels of Figure 6G–I. In this case, the deviations of the dynamic structures resulting from the simulations are of nearly the same magnitude as those observed for panels (D–F), where PDB:3SN6 was considered as a reference structure. This arises from the structurally similar fragments of the loops and intracellular ends of the helices present in the reference structures considered; both of them can be considered as "active" conformers. Minor difference between corresponding RMSD distribution results from the slightly divergent geometries of ICL3, ICL2 (to a lesser extent) and the corresponding sections of the helices. Furthermore, both the structures induced by the presence of either (R,R)-MNFen or (R,S)-MNFen exhibit the same tendency of the distance from the "active" conformer of the receptor. This suggests that the observed conformational changes of the intracellular fragments of the receptor may also influence β-arrestin coupling.

Unfortunately, there is a lack of structural data regarding the structure of β_2-AR bound to the Gi protein, which prevents a more direct verification of the hypothesis about the increased structural similarity of such a state to our data generated for the β_2-AR-(R,S)-NMFen complex.

The RMSF analysis (Figure 6) demonstrates that nearly all TM regions are stabilized upon binding of (R,S)-MNFen, in comparison to (R,R)-MNFen. The most reduced magnitude of fluctuation can be ascribed to TM4, TM5, TM6, and TM7; the latter three regions are associated with the largest differences in molecular conformation of intracellular parts. The mobility of the loop containing Lys305 is also significantly reduced as a consequence of disturbed equilibrium within the corresponding ionic-bridge. Moreover, larger conformational mobility of the loop-neighboring fragment of TM7 observed in the case (R,R)-MNFen-containing complex may be a consequence of the direct contact of the Trp313 sidechain with both ligand and TM1.

From a mechanistic perspective, the structural divergences present in the intracellular part of β_2-AR can be traced back to the stabilizing influence of the ligand, exerted in the binding cavity. This is attained by the above-described alterations in the Trp313-TM7 and Lys305-Asp192 interactions. Reduced mobility in the extracellular region of the receptor is propagated along the receptor domains and shifts the dynamic, conformational equilibrium of the intracellular parts. Interestingly, the larger mobility of the TM regions neighboring to the ligand binding site translates into reduced structural fluctuations of the intracellular parts of the receptor. The latter is demonstrated by the differences in variances of the RMSD parameter distribution calculated either for (R,R)-MNFen- or (R,R)-MNFen-bound receptor (Figure 6).

Notably, the magnitude of the ligand-protein interaction energy is more negative (i.e., more favorable) in the case of (R,S)-MNFen (by ca. 20 kJ/mol) in comparison to (R,R)-MNFen. This finding additionally supports the claim about effect of (R,S)-MNFen stabilizing the conformation of extracellular regions of β_2-AR not only through modifying the internal pattern of residue–residue interactions with the receptor but also through more intensive ligand–protein interactions. It is also worth noting that such energy of interaction is not equivalent to ligand–receptor affinity (mentioned in section 3.2) as it lacks the entropic contribution.

Apart from the above-described findings, we also have discovered some structural rearrangements occurring within the intracellular regions of TM5 and TM6 of the (R,S)-MNFen-bound receptor. They involve the increase of the distance between TM6 and TM7 and seem to be correlated with the disruption of the ionic bridge between Glu268 (TM6) and Lys227 (TM5). This triggers loosening contacts between TM5 and TM6 and reorientation of the Arg328 sidechain, which moves away from Thr274 (TM6). After this series of molecular events, the Glu268-Lys227 ionic bridge is established again. However, Arg328 remains in its newly adopted orientation, increasing the distance between TM6 and TM7 in comparison to both the initial configuration and the (R,R)-MNFen-β_2-AR complex.

So far, the results described in this subsection concerned the comparison of the behavior of β_2-AR complexes containing both stereoisomers of MNFen. To confirm the mechanism of changes in the intracellular part of the receptor suggested earlier, it is worth taking a closer look at the conformational reorganizations occurring in one of the studied systems, that is, the one containing (R,S)-MNFen. As mentioned above, this system exhibits a reorientation of the key methoxynaphthyl group, which, only after some time from the start of the simulation, shows interactions suspected to be the cause of further conformational changes in the receptor. Therefore, it can be expected that before this key change, the conformation of intracellular fragments will resemble that characteristic of the complex with (R,R)-MNFen. To test this, we conducted

a time-dependent analysis of distances between the extreme intracellular fragments of all helices (excluding H8, giving a total of 21 individual pairs), and then examined which of these changes correlated most strongly with the changing conformation of the methoxynaphthylphenyl group of (R,S)-MNFen (expressed by the value of the N-C_1-C_2-C_3 torsion angle; see Figure 4). Furthermore, we also examined the analogous correlation between the value of the aforementioned torsion angle and the mutual orientation of TM1, TM2, and TM7 (see Figure 7B). The results are illustrated in Figure 7.

It was found that the absolute values of the correlation coefficient (R) between the torsion angle values and the studied receptor conformation descriptors range widely, from 0.05 to 0.68. The distances for which $|R| > 0.3$ include 7 cases, which are symbolically illustrated in Figure 7A. It should be noted that a negative correlation corresponds to an increase in the distance between domain fragments occurring with the irreversible conformational change of the ligand group, while a positive correlation corresponds to a decrease in such a distance. The cases with the highest correlations are illustrated in Figure 7C–E. The direction of the largest changes in the extracellular part, in terms of magnitude, is analogous to what was discussed earlier and concerns the distances between the fragments of TM5 and TM7, TM1 and TM6, TM6, and TM7, as well as TM1 and TM5; all these changes correspond to an increase in the distance between the analyzed receptor fragments. Only the next two changes in terms of magnitude (distances for TM1-TM4 and TM2-TM4 pairs) correspond to a decrease in the respective values. From the qualitative analysis of changes presented in Figure 7A, it can be seen that a group of intracellular fragments of the TM1, TM2, and TM7 domains moves closer to TM4 while simultaneously moving further away from TM5 and TM6.

The occurring changes not only involve a shift in the preferred mean distances between domains in the intracellular part, but also an alteration in the size of the conformational space explored by the system, as illustrated in Figure 8C–E. The range of sampled interdomain distances (in other words: the variance associated with the distribution of the respective values) is much larger for systems after the ligand's conformational change. It can thus be stated that the increase in the mean values discussed above is correlated with an increase in the conformational flexibility of the respective fragments. The opposite situation (a decrease in flexibility) may occur in the case of domain fragments for which a decrease in distance was observed, but in this case, this rule does not always apply. (Qualitative data for individual cases are shown in Figure 8).

It is worth noting that the observed changes do not concern the distance between TM3 and TM6, which is often used as a descriptor for the activation process [31, 33, 64]; this variable, regardless of the stereoconfiguration of the bound ligand, corresponds to the value characteristic of the active receptor.

The present results cannot be fully and directly compared to existing literature reports concerning the mechanism of biased signaling, which are usually reported in the context of G-protein bias vs. β-arrestin bias. Additionally, as noted earlier, the structure corresponding to the receptor in complex with Gi protein is not known, making it impossible to quantitatively compare the observed conformational changes with such a hypothetical structure. Nonetheless, in the context of general qualitative comparisons, it is worth observing that the observed changes differ from those distinguishing a G-biased conformation relative to the inactive conformation, specifically the outward shifts of TM6 and TM7 in the intracellular domain [31]. In the present case, the characteristic distance between TM2 and TM7 is practically independent of the type of bound ligand. The observed changes in the distances between domains also do not directly correlate with the conformation characteristic of β-arrestin binding, that is, the reduction in the distance between TM2 and TM7. However, a similar change is the slight outward movement of TM6 [31], which correlates with a slightly greater compatibility of the structure induced by the binding of (R-S)-MNFen with the conformer that binds β-arrestin compared to the one binding Gs (see Figure 6).

In reference to the information from the study [31], it is worth noting that the changes in distances between domains, according to the current results, are characteristic of Gi protein binding and correspond even more to an open conformation with a large intracellular cavity compared to conformers compatible with Gs protein and, to an even greater extent, β-arrestin.

It is also worth noting that we did not observe any inward movements of TM6, which, on the other hand, were observed in simulations of mutated receptors for systems theoretically compatible with both Gs and β-arrestin binding [32].

Regarding the descriptors describing the relative position of the helices (these were dihedral angles defined by quadruplets of fragments of neighboring helices belonging to both intracellular and extracellular parts), no such evident correlations were observed as in the previously discussed case; the strongest correlation ($R = 0.302$) is illustrated in Figure 8F. This indicates that the changes induced by the presence of a ligand with a given stereochemistry do not involve the relative orientation of entire helices but only the position of their intracellular fragments.

All the changes described above may also translate into the conformation of the intracellular loops, as shown in references [65–68] also play a significant role in the process of protein binding in the intracellular part of the receptor. While it can be assumed that shifts in the intracellular fragments of the domains may influence the conformation of the associated loops and, thus, affect the binding of G proteins and arrestins, this effect is extremely difficult to model due to the fact that: (1) The timescale of loop-inherent conformational changes is large and may exceed the microsecond range; the timescale available within atomistic simulations is therefore insufficient to reliably sample the associated conformational equilibria. (2) Due to the significant mobility of the loops and the lack of experimental information on their dominant structure, additional assumptions must be made when modeling the initial conformation. This can be prone to error and serve as a source of additional bias in the simulations. Hence, in this study, we observe the possible connection between the conformational changes in the intracellular part of the receptor described above and the dynamic conformation of the loops, but we are unable to quantitatively determine the nature of this relationship.

3.5 | Coarse-Grained Simulations and Their Results

The main goal of the CG modeling was to verify the reproducibility of the most significant results obtained from atomic simulations described in sections 3.2–3.4. At this stage of the research, we relied on assumptions based on the results of atomic simulations, indicating the dependence of the conformations of selected molecular switches on the type (more specifically, the stereoconfiguration) of the ligand. Since modeling the conformational changes of the receptor induced by the presence of a ligand at the CG level can be problematic or even impossible, the presence of a ligand with a given stereoconfiguration was implicitly represented through appropriate constraints introduced into the model. Specifically, the values were provided in the Methods section, and the conformations resulting from the constraints are illustrated in Figure 8. Furthermore, the Martini 3 force field, with higher-order structures modeled using the GōMartini approach, allows at least a partial representation of the natural changes in protein conformations.

The analysis of the CG simulations included determining the average distances between the intracellular ends of the transmembrane domains, limited to six combinations corresponding to those pairs of domains that were identified based on atomic simulations as being most susceptible to changes in mutual positioning dependent on the ligand's stereoconfiguration (see Figures 7 and 8C–E).

The results are illustrated in Figure 8D, whereas Figure 8C includes the analogous data from atomic simulations corresponding to the trajectories of the receptor complex with (R,R)-MNFen (the entire trajectory) and (R,S)-MNFen (the trajectory from the time of reorientation of the methoxynaphthyl group). Regardless of the resolution of the model used in the simulations, the changes in average distances between the domain fragments are not large and are approximately equal to 0.1–0.2 nm. The standard deviation values (corresponding to the magnitude of fluctuation of a given conformational descriptor) are always increased in the case of (R,R)-MNFen-containing complex in comparison to the (R,S)-MNFen-one; this is in line with observations made in previous section. Additionally, it is worth noting the similar values obtained from atomic and CG simulations, which serve as additional validation of the latter model and confirm that it can accurately represent the structure of the receptor, including the spatial relationships between the domains. The most important observation from this stage of the research is the qualitative (and largely quantitative) agreement in the trends of changes in the intracellular fragments of the receptor induced by the presence of a ligand with a given stereoconfiguration, for both the atomic and CG models. In particular, these changes are consistent in direction with those illustrated in Figure 7 and, for the distances between pairs TM5 and TM7, in Figure 5E. The differences between the predictions of both models are illustrated in Figure 8E.

The high degree of agreement between the predictions of the two independent models, operating at different levels of resolution, validates the results described in the previous section and also provides insight into the mechanism of allosteric communication. Namely, since the CG model is able to reproduce the same effect as the atomic model, the most likely mechanism of signal propagation involves alterations in the interaction strength between TM7 and TM1, as well as between the ligand and TM1 and TM2. According to the mechanistic aspects of β_2-AR (and other GPCRs) activation, stronger, attractive interactions within the extracellular part result in the expansion of the receptor structure in the intracellular part. A similar effect, albeit on a significantly smaller scale, is observed in the current studies.

3.6 | Comparison With the Structural Data

In addition to the above-described analysis of MD simulation results, we also investigated all available experimentally resolved structures of the β_2-AR receptor in the PDB database. The analysis primarily focused on the conformational states of the Trp313 residue and the Lys305-Asp192 ionic lock. Out of 42 available structures, only 2 exhibit configurations of the side chain of Trp313 that are different from the default. These are PDB: 3KJ6 and PDB: 7DHR, corresponding to the inactive and active conformations of the receptor, respectively. In the case of structure 3KJN, the Trp313 rotamer shows a dihedral angle N-C_α-C_β-C_γ value of approximately 170°, close to that observed in simulations of the β_2-AR-(R,R)-MNFen complex and clearly corresponding to the same rotameric state. However, this structure does not contain the ligand molecule (as well as the entire extracellular part of the receptor), allowing the investigation of potential ligand-Trp313 interactions responsible for the different conformation of the considered side chain.

On the other hand, for structure 7DHR, a different rotameric state of Trp313 can be observed, distinct from those observed in simulations and other experimental structures, characterized by a changed rotation around the C_β-C_γ bond. Unfortunately, for both of these structures, receptor parts containing the complete structure of the Lys305-Asp192 ionic lock are not available, preventing the assessment of whether the altered rotameric state of Trp313 correlates with the state of the ionic lock.

As indicated by the current results, conformational changes in both the intracellular and extracellular parts depend, among other factors, on the ligand's contact with residues on TM2. In terms of the possibility of such contact, the ligand (R,S)-MNFen is unique compared to the ligands present in the crystallized structures of β_2-AR. Specifically, due to the large size of the relevant substituent, its possible rotation, and inherent conformational properties, (R,S)-MNFen is the only one capable of exhibiting close contact with residues on TM2, including Ile94 (with a distance from C_α of about 0.5 nm) and Gly90 (0.4 nm). Excluding the two cases of ligands designed to form a covalent bond with mutated residues on TM2 (PDB: 3PDS and PDB: 4QKX), none of the other molecules present in the binding pockets of β_2-AR come close to these values. The corresponding distances typically range from 0.7 to 0.9 nm, and these fragments of the system do not show direct contact.

In reference to the above observations, it can also be speculated that the low number of alternative conformers of the Trp313 side chain (linked in this study to Gi-biased signaling) is related to the unavailability of receptor structures bound to the Gi protein. The available structures only contain the Gs protein, arrestin, other proteins, or are in an unbound state.

Examination of all 42 β_2-AR receptor structures confirms that the ionic lock exhibits much greater conformational variability compared to Trp313. 13 of these structures show no direct contact between the sidechains of Lys305 and Asp192 (e.g., PDB: 6KR8 [all substructures], 6MXT, 5X7D, 3SN6, or 3P0G), mostly due to the flexible side chain of Lys305 interacting with ligands, similar to the effect observed in current simulations. However, it is worth noting that not all structures have parts that are elements of the examined ionic lock.

In addition to the analysis of conformational states, it is noteworthy that the side chain of Trp313 may serve as a binding site for unsaturated aliphatic compounds present in the lipid membrane, as suggested by structures such as 4LDL, 4LDE, 4QKX, or 6 N48, containing enoate compounds interacting with the aromatic ring of Trp313 (in the most common orientation) through CH-π and/or π-π interactions. Furthermore, according to simulation results reported in ref. [69], Trp313 may also participate in binding cholesterol molecules between TM1 and TM7. Although such interactions were not considered in the current simulations, it should be emphasized that they may be relevant in the broader context of Trp313 conformation and its impact on biased agonism.

4 | Conclusions

We have performed long (1 μs-long) molecular dynamics (MD) simulations of β_2-AR in complex with two different stereoisomers of methoxynaphtyl fenoterol (MNFen). The motivation was the experimentally observed phenomenon called the biased agonism [4–8] and associated with preferential activation of a G_s- or β-arrestin-mediated signaling pathway through β_2-AR. The current study relies on (R,R)-MNFen and (R,S)-MNFen, that is, a pair of compounds of extremely similar molecular structure, differing only by stereoconfiguration of a single chiral centre. Yet, they still produce qualitatively different cellular responses [70]. The selection of these ligands provides an opportunity to explore the molecular underpinnings of biased agonism, minimizing the influence of other potentially significant factors associated with the molecular characteristics of a given ligand, which, upon incorporation into the molecular model, could impact the observed activation process. The unbiased MD simulations revealed slightly different interaction patterns of the two considered stereoisomers with binding cavity. The presence of (R,S)-MNFen induced several shifts in conformational dynamics of selected sidechains. The most substantial ones include the change of the rotameric state of the Trp313 sidechain and disturbed equilibria in the Lys305-Asp192 ionic lock. These changes propagate toward the intracellular part of β_2-AR, where they trigger structural response different to that observed in the case of (R,R)-MNFen-bound receptor. In general, the presence of (R,S)-MNFen stabilizes the conformation of extracellular parts of the receptor and increases the conformational heterogeneity of the intracellular fragments, whereas the effect induced by (R,R)-MNFen is opposite. Changes in the structure of the intracellular fragments of the transmembrane domains indicate an increase in the distance between TM1 and TM5, TM5 and TM7, and TM6 and TM7 (of magnitude of ca. 0.2 nm), while there is a slighter distance decrease between the TM1 and TM4, as well as TM2 and TM4 domains. As confirmed in independent simulations at CG resolution, these changes are associated with the interaction of the ligand with Trp313 and a series of other residues on TM1. The dynamic structure of the intracellular regions is closer to both the "G_s-compatible" and "β-arrestin-compatible" ones (defined by the PDB:3SN6 and PDB:6NI3, respectively) in the case of (R,R)-MNFen-containing complex; however, both (R,R)-MNFen and (R,S)-MNFen induce structural responses equally distance from the inactive conformation (defined by PDB:2RH1). In summary, the presented results point out the possible role of Trp313 as well as the Lys305-Asp192 ionic bridge in the ligand-induced structural basis of the biased agonism phenomenon.

Author Contributions

Wojciech Plazinski: conceptualization, methodology, validation, formal analysis, investigation, software, data curation, writing – original draft, writing – review and editing, visualization, supervision. **Aneta Archala:** data curation, writing – original draft. **Krzysztof Jozwiak:** conceptualization, writing – original draft, supervision. **Anita Plazinska:** methodology, validation, formal analysis, investigation, data curation, writing – original draft, writing – review and editing, visualization, project administration, funding acquisition.

Acknowledgments

The authors have nothing to report.

Ethics Statement

The authors have nothing to report.

Conflicts of Interest

The authors declare no conflicts of interest.

Data Availability Statement

The raw data that support the findings of this study (MD trajectories, input files) are available on request from the corresponding author. Other data are available within the paper.

References

1. V. V. Gurevich and E. V. Gurevich, "The Molecular Acrobatics of Arrestin Activation," *Trends in Pharmacological Sciences* 25, no. 2 (2004): 105–111.

2. M. Seyedabadi, M. Gharghabi, E. V. Gurevich, and V. V. Gurevich, "Receptor-Arrestin Interactions: The GPCR Perspective," *Biomolecules* 11, no. 2 (2021): 1–25.

3. P. Y. Jean-Charles, S. Kaur, and S. K. Shenoy, "G Protein-Coupled Receptor Signaling Through β-Arrestin-Dependent Mechanisms," *Journal of Cardiovascular Pharmacology* 70, no. 3 (2017): 142–158.

4. E. Khoury, S. Clément, and S. A. Laporte, "Allosteric and Biased G Protein-Coupled Receptor Signaling Regulation: Potentials for New Therapeutics," *Frontiers in Endocrinology* 5 (2014): 68.

5. J. Shonberg, L. Lopez, P. J. Scammells, A. Christopoulos, B. Capuano, and J. R. Lane, "Biased Agonism at G Protein-Coupled Receptors: The Promise and the Challenges–a Medicinal Chemistry Perspective," *Medicinal Research Reviews* 34, no. 6 (2014): 1286–1330.

6. D. Wootten, A. Christopoulos, M. Marti-Solano, M. M. Babu, and P. M. Sexton, "Mechanisms of Signalling and Biased Agonism in G Protein-Coupled Receptors," *Nature Reviews Molecular Cell Biology* 19, no. 10 (2018): 638–653.

7. M. Ippolito and J. L. Benovic, "Biased Agonism at β-Adrenergic Receptors," *Cellular Signalling* 80 (2021): 109905.

8. K. Jóźwiak and A. Płazińska, "Structural Insights Into Ligand-Receptor Interactions Involved in Biased Agonism of G-Protein Coupled Receptors," *Molecules (Basel, Switzerland)* 26, no. 4 (2021): 851.

9. D. S. Eiger, U. Pham, J. Gardner, C. Hicks, and S. Rajagopal, "GPCR Systems Pharmacology: A Different Perspective on the Development of Biased Therapeutics," *American Journal of Physiology. Cell Physiology* 322, no. 5 (2022): C887–C895.

10. M. Joshi, S. V. Nikte, and D. Sengupta, "Molecular Determinants of GPCR Pharmacogenetics: Deconstructing the Population Variants in β2-Adrenergic Receptor," *Advances in Protein Chemistry and Structural Biology* 128 (2022): 361–396.

11. P. Kolb, D. M. Rosenbaum, J. J. Irwin, J. J. Fung, B. K. Kobilka, and B. K. Shoichet, "Structure-Based Discovery of β 2 -Adrenergic Receptor Ligands," *Proceedings of the National Academy of Sciences of the United States of America* 106, no. 16 (2009): 6843–6848.

12. C. K. Billington, R. B. Penn, and I. P. Hall, "β2 Agonists," *Handbook of Experimental Pharmacology* 237 (2017): 23–40.

13. E. Oliver, F. Mayor, Jr., and P. D'Ocon, "Beta-Blockers: Historical Perspective and Mechanisms of Action," *Revista Española de Cardiología (English Edition)* 72, no. 10 (2019): 853–862.

14. R. J. Lefkowitz, J. Inglese, W. J. Koch, J. Pitcher, H. Attramadal, and M. G. Caron, "G-Protein-Coupled Receptors: Regulatory Role of Receptor Kinases and Arrestin Proteins," *Cold Spring Harbor Symposia on Quantitative Biology* 1, no. 57 (1992): 127–133.

15. M. T. Drake, J. D. Violin, E. J. Whalen, J. W. Wisler, S. K. Shenoy, and R. J. Lefkowitz, "Beta-Arrestin-Biased Agonism at the Beta2-Adrenergic Receptor," *Journal of Biological Chemistry* 283, no. 9 (2008): 5669–5676.

16. R. P. Xiao, X. Ji, and E. G. Lakatta, "Functional Coupling of the Beta 2-Adrenoceptor to a Pertussis Toxin-Sensitive G Protein in Cardiac Myocytes," *Molecular Pharmacology* 47, no. 2 (1995): 322–329.

17. A. Y. H. Woo, T. B. Wang, X. Zeng, et al., "Stereochemistry of an Agonist Determines Coupling Preference of β2-Adrenoceptor to Different G Proteins in Cardiomyocytes," *Molecular Pharmacology* 75, no. 1 (2009): 158–165.

18. V. Cherezov, D. M. Rosenbaum, M. A. Hanson, et al., "High-Resolution Crystal Structure of an Engineered Human β2-Adrenergic G Protein-Coupled Receptor," *Science* 318, no. 5854 (2007): 1258–1265.

19. D. M. Rosenbaum, C. Zhang, J. A. Lyons, et al., "Structure and Function of an Irreversible Agonist-β2 Adrenoceptor Complex," *Nature* 469, no. 7329 (2011): 236–240.

20. S. G. F. Rasmussen, H. J. Choi, J. J. Fung, et al., "Structure of a Nanobody-Stabilized Active State of the β2 Adrenoceptor," *Nature* 469, no. 7329 (2011): 175–180.

21. S. G. F. Rasmussen, B. T. Devree, Y. Zou, et al., "Crystal Structure of the β2 Adrenergic Receptor–Gs Protein Complex," *Nature* 477, no. 7366 (2011): 549–555.

22. A. M. Ring, A. Manglik, A. C. Kruse, et al., "Adrenaline-Activated Structure of β2-Adrenoceptor Stabilized by an Engineered Nanobody," *Nature* 502, no. 7472 (2013): 575–579.

23. M. Bermudez and A. Bock, "Does Divergent Binding Pocket Closure Drive Ligand Bias for Class A GPCRs?," *Trends in Pharmacological Sciences* 40, no. 4 (2019): 236–239.

24. Q. Zhou, D. Yang, M. Wu, et al., "Common Activation Mechanism of Class a GPCRs," *eLife* 8 (2019): 50279.

25. Y. Wu, L. Zeng, and S. Zhao, "Ligands of Adrenergic Receptors: A Structural Point of View," *Biomolecules* 11, no. 7 (2021): 936.

26. J. W. Wisler, S. M. DeWire, E. J. Whalen, et al., "A Unique Mechanism of β-Blocker Action: Carvedilol Stimulates β-Arrestin Signaling," *National Academy of Sciences of the United States of America* 104, no. 42 (2007): 16657–16662.

27. S. Rajagopal, S. Ahn, D. H. Rominger, et al., "Quantifying Ligand Bias at Seven-Transmembrane Receptors," *Molecular Pharmacology* 80, no. 3 (2011): 367–377.

28. D. R. Weiss, S. Ahn, M. F. Sassano, et al., "Conformation Guides Molecular Efficacy in Docking Screens of Activated β-2 Adrenergic G Protein Coupled Receptor," *ACS Chemical Biology* 8, no. 5 (2013): 1018–1026.

29. A. Ishchenko, B. Stauch, G. W. Han, et al., "Toward G Protein-Coupled Receptor Structure-Based Drug Design Using X-Ray Lasers," *International Union of Crystallography* 6, no. 6 (2019): 1106–1119.

30. M. Masureel, Y. Zou, L. P. Picard, et al., "Structural Insights Into Binding Specificity, Efficacy and Bias of a β2AR Partial Agonist," *Nature Chemical Biology* 14, no. 11 (2018): 1059–1066.

31. J. Chen, J. Liu, Y. Yuan, X. Chen, F. Zhang, and X. Pu, "Molecular Mechanisms of Diverse Activation Stimulated by Different Biased Agonists for the β2-Adrenergic Receptor," *Journal of Chemical Information and Modeling* 62, no. 21 (2022): 5175–5192.

32. M. K. Madhu, K. Shewani, and R. K. Murarka, "Biased Signaling in Mutated Variants of β2-Adrenergic Receptor: Insights From Molecular Dynamics Simulations," *Journal of Chemical Information and Modeling* 64, no. 2 (2024): 449–469.

33. R. O. Dror, D. H. Arlow, P. Maragakis, et al., "Activation Mechanism of the β2-Adrenergic Receptor," *National Academy of Sciences of the United States of America* 108, no. 46 (2011): 18684–18689.

34. R. Nygaard, Y. Zou, R. O. Dror, et al., "The Dynamic Process of β2-Adrenergic Receptor Activation," *Cell* 152, no. 3 (2013): 532–542.

35. A. Ranganathan, R. O. Dror, and J. Carlsson, "Insights Into the Role of Asp792.50 in β2 Adrenergic Receptor Activation From Molecular Dynamics Simulations," *Biochemistry* 53, no. 46 (2014): 7283–7296.

36. X. Xiao, X. Zeng, Y. Yuan, et al., "Understanding the Conformation Transition in the Activation Pathway of β2 Adrenergic Receptor via a Targeted Molecular Dynamics Simulation," *Physical Chemistry Chemical Physics* 17, no. 4 (2014): 2512–2522.

37. I. G. Tikhonova, B. Selvam, A. Ivetac, J. Wereszczynski, and J. A. McCammon, "Simulations of Biased Agonists in the β2 Adrenergic Receptor With Accelerated Molecular Dynamics," *Biochemistry* 52, no. 33 (2013): 5593–5603.

38. K. Jozwiak, C. Khalid, M. J. Tanga, et al., "Comparative Molecular Field Analysis of the Binding of the Stereoisomers of Fenoterol and Fenoterol Derivatives to the β2 Adrenergic Receptor," *Journal of Medicinal Chemistry* 50, no. 12 (2007): 2903–2915.

39. M. T. Reinartz, S. Kälble, T. Littmann, et al., "Structure-Bias Relationships for Fenoterol Stereoisomers in Six Molecular and Cellular Assays at the β2-Adrenoceptor," *Naunyn-Schmiedeberg's Archives of Pharmacology* 388, no. 1 (2015): 51–65.

40. M. D. Hanwell, D. E. Curtis, D. C. Lonie, T. Vandermeerschd, E. Zurek, and G. R. Hutchison, "Avogadro: An Advanced Semantic Chemical Editor, Visualization, and Analysis Platform," *Journal of Cheminformatics* 4, no. 8 (2012): 1–17.

41. A. K. Rappé, C. J. Casewit, K. S. Colwell, W. A. Goddard, and W. M. Skiff, "UFF, a Full Periodic Table Force Field for Molecular Mechanics and Molecular Dynamics Simulations," *Journal of the American Chemical Society* 114, no. 25 (1992): 10024–10035.

42. O. Trott and A. J. Olson, "AutoDock Vina: Improving the Speed and Accuracy of Docking With a New Scoring Function, Efficient Optimization, and Multithreading," *Journal of Computational Chemistry* 31, no. 2 (2010): 455–461.

43. J. Eberhardt, D. Santos-Martins, A. F. Tillack, and S. Forli, "AutoDock Vina 1.2.0: New Docking Methods, Expanded Force Field, and

Python Bindings," *Journal of Chemical Information and Modeling* 61, no. 8 (2021): 3891–3898.

44. M. J. Abraham, T. Murtola, R. Schulz, et al., "GROMACS: High Performance Molecular Simulations Through Multi-Level Parallelism From Laptops to Supercomputers," *SoftwareX* 1–2 (2015): 19–25.

45. J. Huang, S. Rauscher, G. Nawrocki, et al., "CHARMM36m: An Improved Force Field for Folded and Intrinsically Disordered Proteins," *Nature Methods* 14, no. 1 (2016): 71–73.

46. S. J. Park, J. Lee, Y. Qi, et al., "CHARMM-GUI Glycan Modeler for Modeling and Simulation of Carbohydrates and Glycoconjugates," *Glycobiology* 29, no. 4 (2019): 320–331.

47. G. Bussi, D. Donadio, and M. Parrinello, "Canonical Sampling Through Velocity Rescaling," *Journal of Chemical Physics* 126, no. 1 (2007): 14101.

48. M. Parrinello and A. Rahman, "Polymorphic Transitions in Single Crystals: A New Molecular Dynamics Method," *Journal of Applied Physics* 52, no. 12 (1981): 7182–7190.

49. R. Hockney, "The Potential Calculation and Some Applications," (1970) Methods Comput. Phys. 135–211.

50. W. L. Jorgensen, J. Chandrasekhar, J. D. Madura, R. W. Impey, and M. L. Klein, "Comparison of Simple Potential Functions for Simulating Liquid Water," *Journal of Chemical Physics* 79, no. 2 (1983): 926–935.

51. B. Hess, "P-LINCS: A Parallel Linear Constraint Solver for Molecular Simulation," *Journal of Chemical Theory and Computation* 4, no. 1 (2008): 116–122.

52. T. Darden, D. York, and L. Pedersen, "Particle Mesh Ewald: An N·Log(N) Method for Ewald Sums in Large Systems," *Journal of Chemical Physics* 98, no. 12 (1993): 10089–10092.

53. S. Miyamoto and P. A. Kollman, "Settle: An Analytical Version of the SHAKE and RATTLE Algorithm for Rigid Water Models," *Journal of Computational Chemistry* 13, no. 8 (1992): 952–962.

54. A. Barducci, G. Bussi, and M. Parrinello, "Well-Tempered Metadynamics: A Smoothly Converging and Tunable Free-Energy Method," *Physical Review Letters* 100, no. 2 (2008): 020603.

55. G. A. Tribello, M. Bonomi, D. Branduardi, C. Camilloni, and G. Bussi, "PLUMED 2: New Feathers for an Old Bird," *Computer Physics Communications* 185, no. 2 (2014): 604–613.

56. A. Barozet, K. Molloy, M. Vaisset, et al., "MoMA-LoopSampler: A Web Server to Exhaustively Sample Protein Loop Conformations," *Bioinformatics* 38, no. 2 (2022): 552–553.

57. P. C. T. Souza, R. Alessandri, J. Barnoud, et al., "Martini 3: A General Purpose Force Field for Coarse-Grained Molecular Dynamics," *Nature Methods* 18, no. 4 (2021): 382–388.

58. M. I. Mahmood, A. B. Poma, and K.-i. Okazaki, "Optimizing Gō-MARTINI Coarse-Grained Model for F-BAR Protein on Lipid Membrane," *Frontiers in Molecular Biosciences [Internet]* 8 (2021): 619381, https://doi.org/10.3389/fmolb.2021.619381/full.

59. P. C. T. Souza, L. Borges-Araújo, C. Brasnett, et al., "GōMartini 3: From Large Conformational Changes in Proteins to Environmental Bias Corrections [Internet]," *bioRxiv* (2024): 589479, https://www.biorxiv.org/content/10.1101/2024.04.15.589479v1.

60. K. Jozwiak, A. Plazinska, L. Toll, et al., "Effect of Fenoterol Stereochemistry on the β2 Adrenergic Receptor System: Ligand-Directed Chiral Recognition," *Chirality* 23, no. 1E (2011): E1–E6.

61. J. Aqvist and J. Marelius, "The Linear Interaction Energy Method for Predicting Ligand Binding Free Energies," *Combinatorial Chemistry & High Throughput Screening* 4, no. 8 (2001): 613–626.

62. P. G. Bolhuis, D. Chandler, C. Dellago, and P. L. Geissler, "Transition Path Sampling: Throwing Ropes Over Rough Mountain Passes, in the Dark," *Annual Review of Physical Chemistry* 53 (2003): 291–318.

63. A. Y. H. Woo, K. Jozwiak, L. Toll, et al., "Tyrosine 308 Is Necessary for Ligand-Directed Gs Protein-Biased Signaling of β2-Adrenoceptor," *Journal of Biological Chemistry* 289, no. 28 (2014): 19351–19363.

64. N. R. Latorraca, A. J. Venkatakrishnan, and R. O. Dror, "GPCR Dynamics: Structures in Motion," *Chemical Reviews* 117, no. 1 (2017): 139–155.

65. S. V. Nikte, M. Joshi, and D. Sengupta, "State-Dependent Dynamics of Extramembrane Domains in the β2-Adrenergic Receptor," *Proteins: Structure, Function, and Bioinformatics* 92, no. 3 (2024): 317–328.

66. F. Sadler, N. Ma, M. Ritt, Y. Sharma, N. Vaidehi, and S. Sivaramakrishnan, "Autoregulation of GPCR Signalling Through the Third Intracellular Loop," *Nature* 615, no. 7953 (2023): 734–741.

67. Y. Han, J. R. D. Dawson, K. R. DeMarco, et al., "Elucidation of a Dynamic Interplay Between a Beta-2 Adrenergic Receptor, Its Agonist, and Stimulatory G Protein," *National Academy of Sciences of the United States of America* 120, no. 10 (2023): e2215916120.

68. O. Ozcan, A. Uyar, P. Doruker, and E. D. Akten, "Effect of Intracellular Loop 3 on Intrinsic Dynamics of Human β2-Adrenergic Receptor," *BMC Structural Biology* 13, no. 1 (2013): 29.

69. X. Cang, Y. Du, Y. Mao, Y. Wang, H. Yang, and H. Jiang, "Mapping the Functional Binding Sites of Cholesterol in β2-Adrenergic Receptor by Long-Time Molecular Dynamics Simulations," *Journal of Physical Chemistry B* 117, no. 4 (2013): 1085–1094.

70. L. Toll, K. Pajak, A. Plazinska, et al., "Binding, Thermodynamics, and Docking of Agonists to the β2-Adrenoceptor Determined Using [3H]-(R,R')-4-Methoxyfenoterol as the Marker Ligand," *Molecular Pharmacology [Internet]* 81 (2012): 846–854.